Analysis of Gating Transitions among the Three Major Open States of the OpdK Channel

Belete R. Cheneke,[†] Bert van den Berg,[‡] and Liviu Movileanu[*,†,§,‖]

[†]Department of Physics, Syracuse University, 201 Physics Building, Syracuse, New York 13244-1130, United States

[‡]Program in Molecular Medicine, University of Massachusetts Medical School, Worcester, Massachusetts 01605, United States

[§]Structural Biology, Biochemistry, and Biophysics Program, Syracuse University, 111 College Place, Syracuse, New York 13244-4100, United States

[‖]Syracuse Biomaterials Institute, Syracuse University, 121 Link Hall, Syracuse, New York 13244, United States

S *Supporting Information*

ABSTRACT: OpdK is an outer membrane protein of the pathogenic bacterium *Pseudomonas aeruginosa*. The recent crystal structure of this protein revealed a monomeric, 18-stranded β-barrel with a kidney-shaped pore, whose constriction features a diameter of 8 Å. Using systematic single-channel electrical recordings of this protein pore reconstituted into planar lipid bilayers under a broad range of ion concentrations, we were able to probe its discrete gating kinetics involving three major and functionally distinct conformations, in which a dominant open substate O_2 is accompanied by less thermodynamically stable substates O_1 and O_3. Single-channel electrical data enabled us to determine the alterations in the energetics and kinetics of the OpdK protein when experimental conditions were changed. In the future, such a semiquantitative analysis might provide a better understanding on the dynamics of current fluctuations of other β-barrel membrane protein channels.
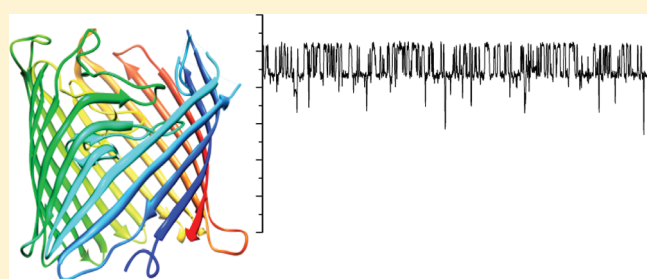
The Gram-negative bacterium *Pseudomonas aeruginosa* utilizes the members of the OprD outer membrane (OM) protein family for the uptake of many small, hydrophilic nutrients required for the growth and function of the cell.[1−9] OpdK is an OprD family member that may be involved in the uptake of vanillate and related aromatic acids.[3,5] The recently reported X-ray crystal structure of the OpdK protein revealed a monomeric, 18-stranded β-barrel with a kidney-shaped transmembrane pore (Figure 1).[10] Van den Berg and colleagues have also reported the X-ray crystal structure of the OprD protein,[11] the archetype of the OprD family, which is implicated in the uptake of positively charged amino acids.[12,13] While the overall structure of the OprD protein is very similar to that of OpdK,[10,11] a striking distinction between these two channels is the conformation of the pore-restricting loop L3. The conformation of this loop in OpdK determines that its constriction is substantially wider than that in OprD (the narrowest diameter is 8.0 Å in OpdK compared to 5.5 Å in OprD, as measured by the side chain to side chain distance).

Current fluctuations observed in single-channel experiments with OM proteins are determined by spontaneous stochastic gating of the pore,[14,15] which is a fundamental feature of most β-barrels.[16−24] The mechanisms by which β-barrel protein pores switch among various well-defined, functionally distinct energetic states are still not well understood.[18,19] Three possible hypotheses were raised for the mechanisms of gating in β-barrel

pores from Gram-negative bacteria: (i) the electrostatic hypothesis, which implies local electrostatic alterations within the eyelet of the pore lumen, precluding ions from crossing the limiting barrier;[16,18,19] (ii) the steric hypothesis, which involves extensive stochastic movements of the long loop L3, occluding the interior of the pore;[11,18,20,23,25,26] (iii) the motions of other large extracellular loops that fold back into the interior of the pore.[21,22,27]

There are various mechanisms that drive spontaneous gating in β-barrel membrane protein pores. Recently, we showed that introducing a pool of negative charges within a robust β-barrel protein pore can induce current fluctuations in the form of well-defined transient current closures, which are otherwise absent in the native protein.[28,29] Conformational fluctuations of the L3 extracellular loop that folds back into the pore lumen is a hallmark in the spontaneous gating of trimeric porins, including the outer membrane proteins C (OmpC) and F (OmpF) of *E. coli*.[20,23,30−33] Liu and Delcour showed that single-site mutations that alter a putative hydrogen bond between loop L3 and the barrel wall, along with ion-pair interactions at the root of the L3 loop impact the spontaneous gating activity of OmpC.[20] While the 16-stranded barrels of OmpC and OmpF have no significant sequence and structural homology to proteins of the
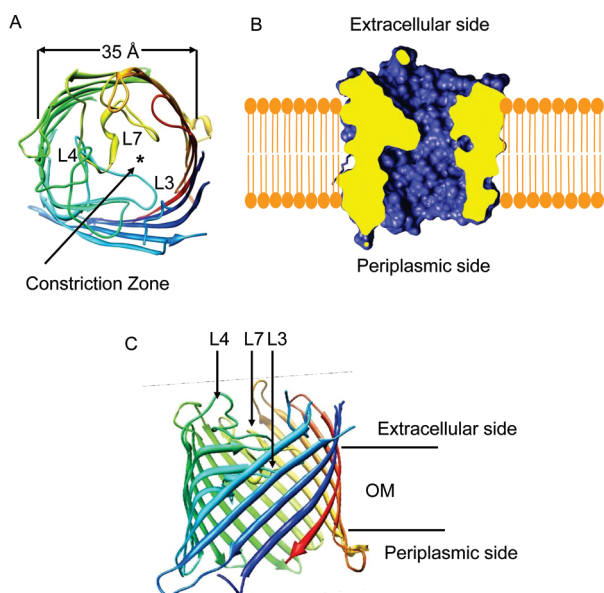
Figure 1. Structural representation of the OpdK protein.[10] (A) A cross-sectional view of the OpdK protein from the extracellular side. The asterisk shows the location of the pore. (B) A cross-sectional view of the lumen of the OpdK protein pore. (C) A view of the OpdK protein revealing the arrangements of the extracellular loops in the direction normal to the lipid bilayer.

OprD family, the inward-folded conformation of loop L3 is, in both protein families, an important contributor to the formation of a narrow channel constriction. Thus, the perturbation of interactions within the interior of β-barrel OM pores is likely to play a general and critical role in determining the frequency of spontaneous channel gating, the duration of the closing events, and the amplitude of the current fluctuations produced by functionally distinct conformations of the obstructing parts of the protein.[23,34]

In the past decade, several groups have employed full-atomistic molecular dynamics (MD) simulations to examine spontaneous stochastic gating of OM proteins from Gram-negative bacteria.[21,35−38] The obvious advantage of computational biophysics studies is the direct inspection of the gating kinetics in OM proteins, which is not achievable with electrophysiological techniques. For example, Faraldo-Gomez and colleagues explored ferric hydroxamate uptake component A (FhuA) of *E. coli* and found that the extracellular loops move as relatively stiff entities relative to the protein lumen.[39] On the other hand, MD studies were recently pursued to reveal enhanced stability of some extracellular loops in β-barrel OM proteins.[40] Therefore, these recent theoretical studies well complemented single-channel electrical recordings with reconstituted proteins into lipid bilayers, illuminating a different type of mechanistic information on the stability and spontaneous stochastic gating of OM proteins.

In this study, we focused on the systematic exploration of the kinetics of the stochastic spontaneous current fluctuations observed with the OpdK protein as a result of the alterations of experimental conditions, such as salt concentration in the chamber and applied transmembrane potential. We employed single-channel electrical recordings to demonstrate that the OpdK protein pore undergoes a kinetic pathway with three major open substates. Methodical analysis of dwell-time histograms of the discrete current fluctuations was used to derive the kinetic rate constants for the transitions of the OpdK protein pore from one

energetic substate to another as well as the corresponding standard free energies. A simple three-state kinetic model and a three-barrier, two-well free energy landscape were used to interpret the current transitions among the three major open substates of the OpdK channel. In addition, we examined electrical recordings collected with loop-deletion OpdK mutants to reveal a better understanding of the impact of long extracellular loops on the single-channel dynamics of the channel.

■ EXPERIMENTAL SECTION

Cloning, Overexpression, and Purification of OpdK. The OpdK gene lacking the part coding for the signal sequence was amplified from genomic DNA of *P. aeruginosa* and was then cloned into the pB22 vector[41] with the *E. coli YtfM* signal sequence at the N-terminus and introducing a 7-His tag at the N-terminus and a TEV protease cleavage site for removal of the His tag. The protein was expressed in C43 (DE3) *E. coli* cells. Cells were grown at 37 °C for 3 h until $OD_{600} \sim 0.6$ and then induced by 0.1% (w/v) arabinose and grown for 3−5 h at 30 °C. Subsequent steps were performed at 4 °C. After harvesting by centrifugation, the cells were resuspended in TSB buffer (20 mM Tris-HCl pH 8.0, 300 mM NaCl, 10% (v/v) glycerol) and ruptured at 15000−20000 psi (1 psi ≈ 6.9 kPa) in a microfluidizer (Avestin Emulsiflex C-3). Total membranes were obtained by centrifugation at 100000*g* for 40 min, after which the pellet was resuspended in 1% LDAO in TSB and stirred for 2 h. This solution was centrifuged at 100000*g* for 30 min, and the supernatant was loaded onto a nickel column (chelating sepharose; GE Healthcare) equilibrated in TSB containing 0.2% LDAO. After washing the column with 15 column volumes 20 mM imidazole in TSB/0.2% LDAO, the protein was eluted with 250 mM imidazole.

The protein was concentrated and loaded on a gel filtration Superdex-200 26/60 chromatography column (Amersham Biosciences), equilibrated in 10 mM Tris/50 mM NaCl/0.05% LDAO pH 8. OpdK containing fractions were pooled and concentrated to ∼0.2 mg/mL. TEV protease was added at a molar ratio of ∼5 (OpdK:TEV), and the protein was incubated at room temperature overnight with gentle rocking. Subsequently, NaCl was added to 300 mM and imidazole to 5 mM, and the solution was loaded onto a small (∼2 mL) nickel column. The column was washed with 5 column volumes buffer containing 5 mM imidazole and combined with the flow through. The pure OpdK protein was concentrated to ∼5 mg/mL (determined by OD_{280}, using a $E_{1\%}$ of 17), aliquotted, and flash-frozen in liquid nitrogen. The purity of the OpdK protein samples was assessed by SDS-PAGE gel electrophoresis (Supporting Information, Figure S1).

Engineering of Loop-Deletion OpdK Mutants. The ΔL3, ΔL4, and ΔL7 loop deletions of the OpdK protein were made by PCR (Expand high fidelity PCR system, Roche) (Supporting Information, Tables S1 and S2). The deletions were made based on inspection of the wild-type OpdK structure (WT-OpdK),[10] with the requirement that the residues immediately before and after the deletion were close enough in space so that they could be replaced by a single glycine residue without introducing large conformational changes and perturbations of other neighboring loops. All deletions were verified by DNA sequencing. Expression and purification of the loop-deletion OpdK mutants were carried out in the same way as for the WT-OpdK protein, including the removal of the N-terminal His-tag by cleavage with TEV protease.

Single-Channel Current Recordings on Planar Lipid Bilayers. Single-channel current measurements were carried out with planar lipid membranes.[42,43] Briefly, both chambers (1.5 mL each) of the bilayer apparatus were separated by a 25 μm thick Teflon septum (Goodfellow Corp., Malvern, PA). An aperture in the septum of $\sim$60 μm diameter was pretreated with hexadecane (Aldrich Chemical Co., Milwaukee, WI) dissolved in highly purified n-pentane (Burdick & Jackson, Allied Signal Inc., Muskegon, MI) at a concentration of 10% (v/v). The standard electrolyte in both chambers was 1000 mM KCl, 10 mM potassium phosphate, pH 8.0, unless otherwise stated. The bilayer was formed with 1,2-diphytanoyl-sn-glycerophocholine (Avanti Polar Lipids Inc., Alabaster, AL). OpdK was added to the cis chamber, which was at ground. Current flow is shown as positive, and it represents a positive charge moving from the $trans$ to cis chamber. Currents were recorded by using an Axopatch 200B patch-clamp amplifier (Axon Instruments, Foster City, CA) connected to the chambers by Ag/AgCl electrodes.[44,45] An Optiplex Desktop Computer (Dell, Austin, TX) equipped with a Digitdata 1440 A/D converter (Axon) was used for data acquisition. The output from this amplifier was also filtered by an 8-pole low-pass Bessel filter (Model 900, Frequency Devices, Haverhill, MA) at a frequency of 10 kHz and sampled at 50 kHz. Acquisition and analysis of data were performed using pClamp 10.2 software (Axon).

The time resolution of the single-channel electrical recordings can be derived using the relationship for the rise time of the filter $T_r = 339/f_c$, where f_c is the corner frequency of the low-pass Bessel filter.[46] For a value of $f_c = 2$ kHz, we obtain $T_r = \sim$170 μs. This value would give us a dead time $T_d = 0.54 \times T_r = 92$ μs. Events shorter than this value were missed. Most of the current transitions were much longer than 100 μs. We estimated that the missed current blockades, under all experimental conditions explored in this work, were not more than 6% of the total number of events in each trace. In addition, the fitted average dwell times were greater than 1 ms, which is well above the time resolution of these measurements. Therefore, we did not introduce corrections for the missed events.[47−49]

■ RESULTS

WT-OpdK Protein Exhibits a Kinetic Pathway with Three Major Open Substates. We adopted an intentionally exploratory approach for examining the biophysical properties of the WT-OpdK protein. The features of the pore gating were investigated when the KCl concentration and the applied transmembrane potential were varied on a systematic basis. Importantly, we needed to remove the 7-His tag at the N-terminus because this engineered polypeptide fragment enhanced the current noise and the frequency of the low-conductance O_1 open substates (Supporting Information, Figure S1). All single-channel data presented in this work were acquired with the 7-His tag-free OpdK protein.

Single-channel data showed that the OpdK protein inserts in both orientations.[10] This conclusion was previously relied on the asymmetry of the single-channel electrical current recorded at identical positive and negative applied transmembrane potentials. However, there is a preference of the OpdK protein to insert more frequently in one direction than in other ($\sim$75% versus $\sim$25%). All our single-channel electrical data presented in this work were collected with the OpdK protein inserted in dominant orientation ($\sim$75%). For example, in 1 M KCl, the
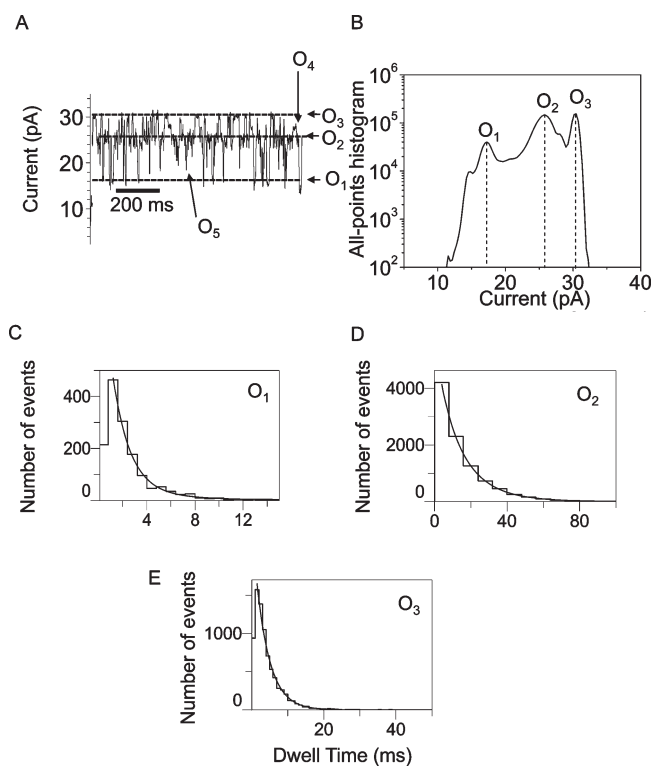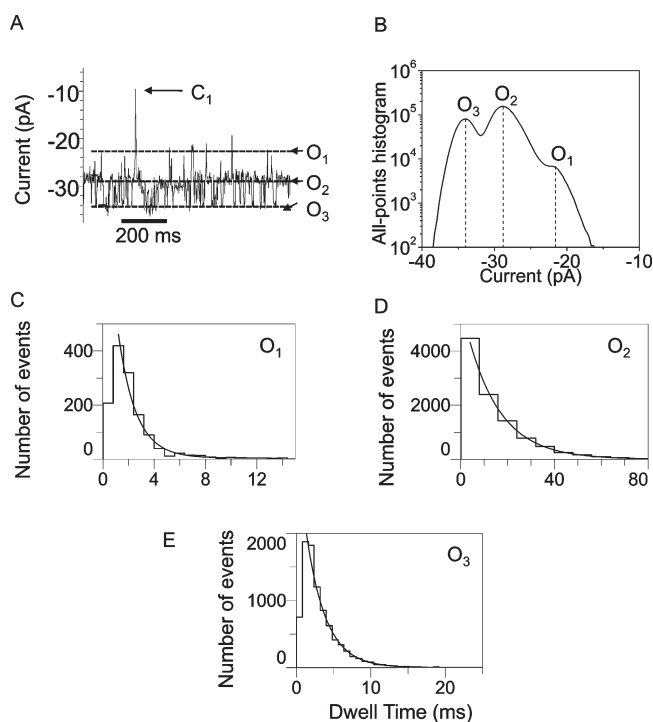

Figure 2. Representative single-channel electrical recordings with the OpdK protein in 1 M KCl and at an applied transmembrane potential of $+80$ mV. (A) Typical single-channel electrical trace recorded at $+80$ mV; (B) all-points current amplitude histogram of collected data from (A); (C) dwell-time histogram of the O_1 events from (A); (D) dwell-time histogram of the O_2 events from (A); (E) dwell-time histogram of the O_3 events from (A). The results of the fits were the following: (C) $\tau_{O1} = 2.5 \pm 0.1$ ms; (D) $\tau_{O2} = 14.3 \pm 0.4$ ms; (E) $\tau_{O3} = 3.7 \pm 0.1$ ms. The fits were based upon a log likelihood ratio (LLR) test with a given confidence level of 0.95.[48−50] For the sake of clarity, the single-channel electrical traces are low-pass Bessel filtered at 200 Hz.

single-channel current corresponding to the most probable O_2 substate and measured at a transmembrane potential of $+80$ mV, under preferred orientation, was 23.5 ± 2.3 pA. At the same time, we recorded a slightly greater current of -27.6 ± 3.5 pA at a transmembrane potential of -80 mV ($n > 5$ distinct determinations), revealing the asymmetry of the observed single-channel current. Vice versa, if a single-channel insertion was characterized by a greater current at a positive voltage bias than at a negative voltage bias, then we assigned that this protein channel adopted the less preferred orientation. This finding is quite different from what we have learned with the trimeric OmpF and OmpC porins, which insert in a single direction with the extracellular opening facing the cis side of the chamber.

In Figures 2−5, we show typical single-channel electrical traces with the WT-OpdK protein recorded under various conditions of KCl concentration and applied transmembrane potential. Clearly, these traces exhibit three distinct major open substate current levels (O_1, O_2, and O_3) that were further explored using standard dwell time and current amplitude histograms. These three major current substates were determined using both all-points current amplitude histograms (Figures 2−5) and standard histograms of fitted current amplitude levels (Supporting Information, Figure S2). The fitted current amplitude histograms were derived using the
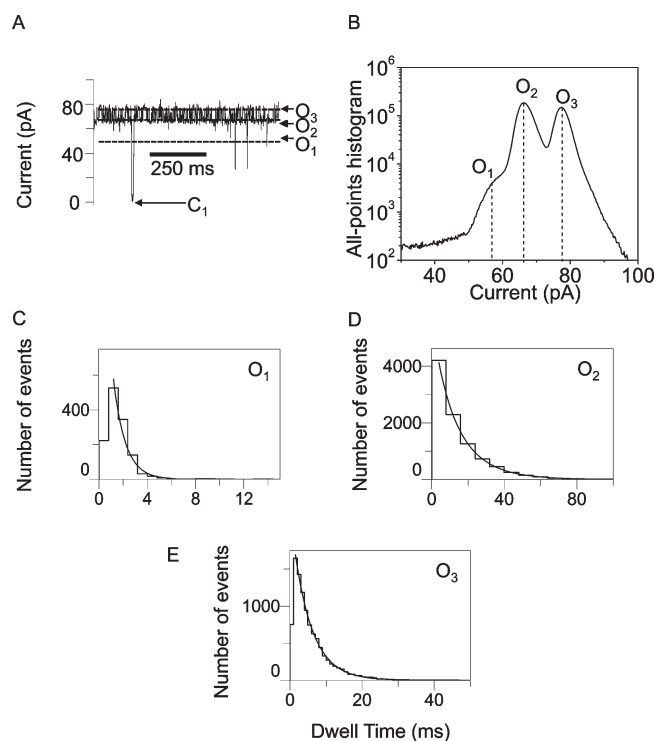
Figure 3. Representative single-channel electrical recordings with the OpdK protein in 1 M KCl and at an applied transmembrane potential of −80 mV. (A) Typical single-channel electrical trace recorded at −80 mV; (B) all-points current amplitude histogram of collected data from (A); (C) dwell-time histogram of the O_1 events from (A); (D) dwell-time histogram of the O_2 events from (A); (E) dwell-time histogram of the O_3 events from (A). The results of the fits were the following: (C) τ_{O1} = 1.5 ± 0.1 ms; (D) τ_{O2} = 14.2 ± 0.3 ms; (E) τ_{O3} = 2.6 ± 0.1 ms. The other conditions are the same as in Figure 2.
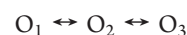
Figure 4. Representative single-channel electrical recordings with the OpdK protein in 4 M KCl and at an applied transmembrane potential of +80 mV. (A) Typical single-channel electrical trace recorded at +80 mV; (B) all-points current amplitude histogram of collected data from (A); (C) dwell-time histogram of the O_1 events from (A); (D) dwell-time histogram of the O_2 events from (A); (E) dwell-time histogram of the O_3 events from (A). The results of the fits were the following: (C) τ_{O1} = 1.2 ± 0.1 ms; (D) τ_{O2} = 8.4 ± 0.4 ms; (E) τ_{O3} = 7.2 ± 0.1 ms. The other conditions are the same as in Figure 2.

ClampFit software. We also observed some substate contamination with additional current levels. For example, a careful inspection of the single-channel electrical recordings in Figures 3A and 4A indicated the presence of closing events (C_1). These current blockades, although quite infrequent as compared with the major open substates O_1, O_2, and O_3 (Figures 2−5; Supporting Information, Figure S2), might be attributed to a closed conformation of the OpdK channel. Using fitted current amplitude histograms (Supporting Information, Figure S2), we estimated that their event probability is smaller than 0.01% of the total number of events. Other observed open substate contaminations were O_4 and O_5. The open O_4 substate was located at approximately halfway between the open O_2 and O_3 substates (Figure 2A; Supporting Information, Figure S2A) and exhibited an event probability smaller than ∼2.6%. The open O_5 substate was located between the open O_1 and O_2 substates (Figure 2A; Supporting Information, Figure S2A) and exhibited an event probability smaller than ∼1.4%. Overall, we found that the three major open substates O_1, O_2, and O_3 occurred with a total event probability of at least 96% of the recorded single-channel events.

The fit of standard dwell-time histograms of all substates contained a well-defined single-exponential function. To determine the number of exponentials for the best fit, we employed the log likelihood ratio (LLR) test to compare different fitting models.[48−50] At a confidence level of 0.95, the best model was single-exponential dwell-time distribution.

Fits to a two-exponential model were not significantly better than single-exponential models, as judged by the LLR value.

Using standard protocols in ClampFit 10.0 software (Axon), we choose three levels corresponding to the three current substates. For positive transmembrane potentials, the levels 0, 1, and 2 were chosen for the O_1, O_2, and O_3 current substates, respectively. Similarly, for negative transmembrane potentials, the levels 0, 1, and 2 were chosen for the open O_1, O_2, and O_3 substates, respectively. pClamp was set to determine all dwell times for the entire recording time of the trace file (τ_{O1}, τ_{O2}, and τ_{O3}; Figures 2−5).

Therefore, single-channel electrical recordings with the WT-OpdK protein revealed three major open substates for all the experimental conditions investigated in this work (Figures 2−5; Supporting Information, Figures S2, S3, and S5). In addition, no O_1 to O_3 or O_3 to O_1 transition was observed in this work (Supporting Information, Figure S3), suggesting a linear kinetic scheme with three distinguishable substates:

$$O_1 \leftrightarrow O_2 \leftrightarrow O_3$$

with the baseline level located on the most probable open substate O_2, from which reversible transitions to the O_1 and O_3 levels can occur. These three major open substates distinguished from the background noise of the channel, as evidenced under of a broad range of conditions, including KCl concentration, voltage, and temperature. For example, a typical
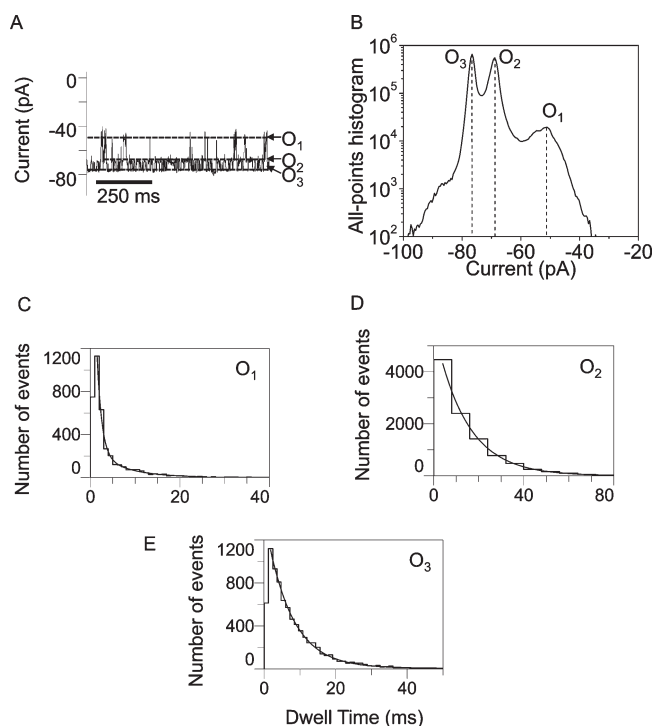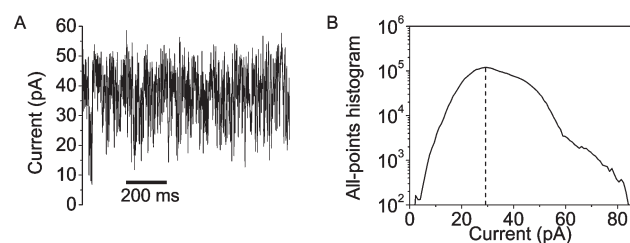
Figure 5. Representative single-channel electrical recordings with the OpdK protein in 4 M KCl and at an applied transmembrane potential of -80 mV. (A) Typical single-channel electrical trace recorded at -80 mV; (B) all-points current amplitude histogram of collected data from (A); (C) dwell-time histogram of the O_1 events from (A); (D) dwell-time histogram of the O_2 events from (A); (E) dwell-time histogram of the O_3 events from (A). The results of the fits were the following: (C) $\tau_{O1} = 3.2 \pm 0.2$ ms; (D) $\tau_{O2} = 8.3 \pm 0.3$ ms; (E) $\tau_{O3} = 5.2 \pm 0.1$ ms. The other conditions are the same as in Figure 2.

Figure 6. Representative single-channel electrical recording acquired with the OpdK ΔL7 protein. (A) Single-channel electrical trace. (B) All-points current amplitude histogram. The single-channel experiments were performed in 1 M KCl, 10 mM potassium chloride, pH 8.0. The transmembrane potential was $+40$ mV.

single-channel current recording acquired at a temperature of 4 °C revealed both the preservation of the number of substates and the absence of the O_1 to O_3 and O_3 to O_1 current transitions (Supporting Information, Figure S3).

The duration of each open substate and its event frequency was strongly dependent on the applied transmembrane potential and the KCl concentration in the chamber (Figures 2–5). Dwell time histograms of all events revealed a total of three exponential time distributions. This finding confirmed the rule that the minimum number of discrete states in a Markov process is equal to the number of exponential components in the probability density functions for those states.[51] Therefore, we have four transition kinetic rates among the three states: $k_{O1\rightarrow O2}$, $k_{O2\rightarrow O1}$, $k_{O2\rightarrow O3}$, and $k_{O3\rightarrow O2}$ for the $O_1 \rightarrow O_2$, $O_2 \rightarrow O_1$, $O_2 \rightarrow O_3$, and $O_3 \rightarrow O_2$ current transitions, respectively.

Single-Channel Electrical Recordings with the Loop-Deletion OpdK Proteins. To better understand the dynamics of the current fluctuations exhibited by the WT-OpdK protein, we performed single-channel electrical recordings with the loop-deletion OpdK mutants. Crystal structure of the native OpdK protein revealed that there are three long, tightly packed extracellular loops, L3, L4, and L7, located near the pore constriction. Therefore, we decided to explore deletions employing these loops. Since these extracellular loops are tightly packed within the pore interior, we designed them in such a way that the residues immediately before and after the deletion were

close enough in space so that they could be replaced by a single Gly residue without introducing a significant conformational change or a perturbation of other loops (Supporting Information, Table S2 and Figure S4). OpdK ΔL3 mutant lacks the region Asp124-Pro129. Importantly, this region of the L3 loop forms two salt bridges, Asp124-Arg16 (between L3 and pore wall, respectively) and Arg126-Glu78 (between L3 and L2, respectively). The second and third deletion-loop OpdK mutants, OpdK ΔL4 and OpdK ΔL7, lack the regions Leu166-Lys175 and Ser281-Gly287, respectively. OpdK ΔL7 also removes a salt bridge, Arg284-Asp116 (between L7 and L3, respectively).

Our single-channel electrical recordings showed no statistically different behavior of OpdK ΔL3 from the native OpdK protein at room temperature (Supporting Information, Figure S5A and Figure S5B). When a single OpdK ΔL4 protein was reconstituted into a planar lipid bilayer, again we observed a three-state discrete single-channel behavior but featured by very short-lived, hardly resolvable current fluctuations between the open O_2 and O_3 substates (Supporting Information, Figure S5C). The current amplitude of the O_2 to O_3 single-channel fluctuations was somewhat smaller than that value observed with the WT-OpdK protein and the OpdK ΔL3 mutant, presumably due to very short current transitions between these substates.

In contrast to the OpdK ΔL3 and OpdK ΔL4 proteins, a dramatic alteration of the channel behavior was found with the OpdK ΔL7 mutant (Figure 6). This mutant exhibited a much greater single-channel conductance than that value measured with the WT-OpdK protein. The all-points current amplitude histogram showed a major peak located at $\sim$725 pS, which is almost double than the single-channel conductance recorded with the WT-OpdK protein under similar conditions (350 pS).[10] In addition, the single-channel electrical signature of the OpdK ΔL7 protein revealed rapid and large-current amplitude fluctuations, indicating a large perturbation of the loop packing within the pore interior. We showed a typical electrical trace recorded with OpdK ΔL7 at $+40$ mV, since this channel became very unstable at greater applied transmembrane potentials (e.g., $+80$ mV).

Analysis of the Kinetic Rate Constants of the Single-Channel Current Fluctuations of the Wild-Type OpdK Protein. Since the major open substates O_1, O_2, and O_3 occurred under all experimental conditions explored in this work and with a total event probability of at least 96%, we adopted a three-state kinetic model for calculating the four rate constants (Supporting Information). We employed the average parameters of event frequency (f) and event dwell time (τ) of the flanked O_1 and O_3

Table 1. Determination of All Kinetic Rate Constants and the Average Dwell Times of the O_2 Substate

| U (mV)[a]	C_{KCl} (M)[a]	$k_{O1\rightarrow O2}$ (s^{-1})	$k_{O2\rightarrow O1}$ (s^{-1})	$k_{O2\rightarrow O3}$ (s^{-1})	$k_{O3\rightarrow O2}$ (s^{-1})	τ_{O2} (ms)[b]	τ_{O2} (ms)[c]
80	1	250 ± 18	18 ± 3	48 ± 24	230 ± 71	11.5 ± 2.4	13.7 ± 2.4
−80	1	180 ± 8	11 ± 2	53 ± 18	250 ± 52	12.5 ± 1.6	14.1 ± 1.9
80	4	642 ± 50	11 ± 5	116 ± 21	151 ± 5	8.1 ± 0.3	8.2 ± 2.1
−80	4	280 ± 9	10 ± 3	94 ± 36	130 ± 11	8.2 ± 0.8	8.1 ± 1.9

[a] The first and second columns indicate the applied transmembrane potential and the KCl concentration in the chamber, respectively. [b] The average dwell times of the O_2 substate are determined from fittings of the standard time histograms. [c] The average dwell times of the O_2 substate are calculated using the event frequencies and average dwell times of the O_1 and O_3 substates (eq 1); Supporting Information.

substates to derive all kinetic rates of the WT-OpdK protein:[52,53]

$$k_{O1 \rightarrow O2} = \frac{1}{\tau_{O1}}$$

$$k_{O2 \rightarrow O1} = \frac{f_{O1}}{1 - f_{O1}\tau_{O1} - f_{O3}\tau_{O3}}$$

$$k_{O2 \rightarrow O3} = \frac{f_{O3}}{1 - f_{O1}\tau_{O1} - f_{O3}\tau_{O3}} \tag{1}$$

$$k_{O3 \rightarrow O2} = \frac{1}{\tau_{O3}}$$

In 1 M KCl concentration and at a transmembrane potential of +80 mV, the single-channel electrical traces revealed large-amplitude current fluctuations that reached an open O_1 substate, with a rate constant $k_{O2\rightarrow O1} = 18 \pm 3$ s^{-1} ($n = 3$ experiments, Table 1). The most probable substate is an open-state current, which is denoted by O_2, with the event rate constants $k_{O1\rightarrow O2} = 250 \pm 18$ s^{-1} and $k_{O3\rightarrow O2} = 230 \pm 71$ s^{-1} ($n = 3$), respectively. Moreover, we observed low-amplitude current transitions that reached a large-conductance open O_3 substate, with a rate constant $k_{O2\rightarrow O3} = 48 \pm 24$ s^{-1} ($n = 3$). The number of major open substates and observable channel transitions is conserved at negative transmembrane potentials. For example, at an applied transmembrane potential of −80 mV, the kinetic rate constant of the O_1 events was $k_{O2\rightarrow O1} = 11 \pm 2$ s^{-1} ($n = 3$). The most probable open O_2 substate occurred with the event rate constants $k_{O1\rightarrow O2} = 180 \pm 8$ s^{-1} and $k_{O3\rightarrow O2} = 250 \pm 52$ s^{-1}, respectively. The large-conductance open O_3 substate events occurred with a kinetic rate constant $k_{O2\rightarrow O3} = 53 \pm 18$ s^{-1} ($n = 3$).

The kinetic rate constants of the low- and large-amplitude current transitions were strongly dependent on the KCl concentration in the chamber. Figures 4 and 5 show representative single-channel electrical data recorded in 4 M KCl. The number of open substates was also conserved with the large alterations in the KCl concentration in the chamber. At a transmembrane potential of +80 mV, the single-channel electrical traces revealed large-amplitude current closures that reached an open O_1 substate with a kinetic rate constant $k_{O2\rightarrow O1} = 11 \pm 5$ s^{-1} ($n = 3$, Table 1). The most frequent open O_2 substate occurred with the event rate constants $k_{O1\rightarrow O2} = 642 \pm 50$ s^{-1} and $k_{O3\rightarrow O2} = 151 \pm 5$ s^{-1} ($n = 3$), respectively. The low-amplitude current transitions that reached a large-conductance open O_3 substate took place with a kinetic rate constant $k_{O2\rightarrow O3} = 116 \pm 21$ s^{-1} ($n = 3$). At a negative transmembrane potential of −80 mV, the event rate constant of the low-conductance open O_1 substate $k_{O2\rightarrow O1} = 10 \pm 3$ s^{-1} ($n = 3$). We observed the most frequent open O_2 substate with the kinetic rate constants $k_{O1\rightarrow O2} = 280 \pm 9$ s^{-1} and $k_{O3\rightarrow O2} = 130 \pm 11$ s^{-1} ($n = 3$), respectively. The large-conductance open O_3 substate occurred with a rate constant $k_{O2\rightarrow O3} = 94 \pm 36$ s^{-1} ($n = 3$).
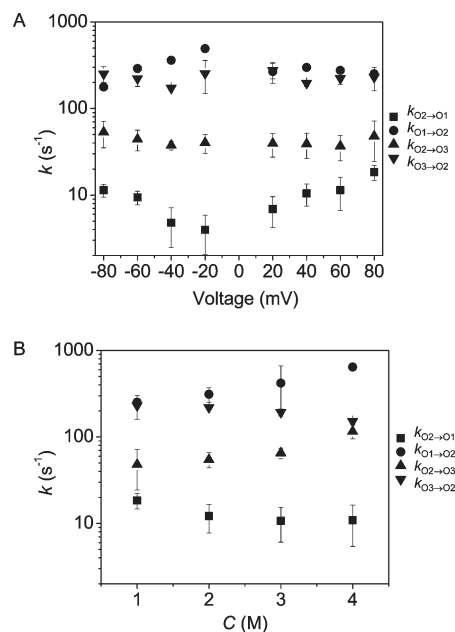
Figure 7. Voltage and salt dependence of the rate constants of the single-channel transitions observed with the OpdK protein. (A) Voltage dependence of the kinetic rate constants in 1 M KCl. (B) KCl concentration dependence of the kinetic rate constants recorded at a transmembrane potential of +80 mV.

The voltage and KCl concentration dependences of the kinetic rates are shown in Figure 7. Remarkably, the kinetic rates $k_{O2\rightarrow O3}$ and $k_{O3\rightarrow O2}$, which involve the transitions $O_2 \leftrightarrow O_3$, are not clearly voltage dependent (Figure 7A). In contrast, the $k_{O2\rightarrow O1}$ rate constant increased with the increase in the absolute value of the applied transmembrane voltage. The $k_{O1\rightarrow O2}$, $k_{O2\rightarrow O3}$, and $k_{O3\rightarrow O2}$ kinetic rate constants were strongly dependent on the KCl concentration in the chamber (Figure 7B). For all experimental conditions explored in this work, we observed that $k_{O1\rightarrow O2} > k_{O2\rightarrow O1}$ and $k_{O3\rightarrow O2} > k_{O2\rightarrow O3}$.

Energetic Parameters for the Single-Channel Current Fluctuations of the WT-OpdK Protein. Using dwell time histograms derived from single-channel electrical recordings (Figures 2−5), we were able to obtain a complete kinetic picture of the dynamics of the OpdK protein pore. All kinetic rate constants $k_{O1\rightarrow O2}$, $k_{O2\rightarrow O1}$, $k_{O2\rightarrow O3}$, and $k_{O3\rightarrow O2}$ for the major $O_1 \rightarrow O_2$, $O_2 \rightarrow O_1$, $O_2 \rightarrow O_3$, and $O_3 \rightarrow O_2$ current transitions, respectively, were calculated using the frequencies and dwell times of the low-conductance open O_1 substate and large-conductance open O_3 substate (eq 1). The direct relationships between the kinetic rate constants and their corresponding
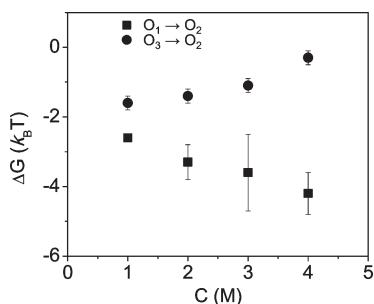
Figure 8. Dependence of the free energies (ΔG) on the KCl concentration in the chamber. The other conditions are the same as in Figure 2.

activation free energies are the following:[54−56]

$$k_{O1 \rightarrow O2} = C_{O1 \rightarrow O2} e^{-\Delta G^{\neq}_{O1 \rightarrow O2}/k_B T}$$
$$k_{O2 \rightarrow O1} = C_{O2 \rightarrow O1} e^{-\Delta G^{\neq}_{O2 \rightarrow O1}/k_B T}$$
$$k_{O2 \rightarrow O3} = C_{O2 \rightarrow O3} e^{-\Delta G^{\neq}_{O2 \rightarrow O3}/k_B T} \quad (2)$$
$$k_{O3 \rightarrow O2} = C_{O3 \rightarrow O2} e^{-\Delta G^{\neq}_{O3 \rightarrow O2}/k_B T}$$

where C coefficients are the frequency factors of the respective transitions. Here, $\Delta G^{\neq}_{O1 \rightarrow O2}$, $\Delta G^{\neq}_{O2 \rightarrow O1}$, $\Delta G^{\neq}_{O2 \rightarrow O3}$, and $\Delta G^{\neq}_{O3 \rightarrow O2}$ are the four corresponding free energies of activation required for the transition from one energetic state to the other, respectively. These parameters permit us to calculate the standard free energies $\Delta G_{O1 \rightarrow O2}$ and $\Delta G_{O3 \rightarrow O2}$:[57,58]

$$\Delta G_{O1 \rightarrow O2} = \Delta G^{\neq}_{O1 \rightarrow O2} - \Delta G^{\neq}_{O2 \rightarrow O1} = -k_B T \ln\left(\frac{k_{O1 \rightarrow O2}}{k_{O2 \rightarrow O1}}\right)$$

$$\Delta G_{O3 \rightarrow O2} = \Delta G^{\neq}_{O3 \rightarrow O2} - \Delta G^{\neq}_{O2 \rightarrow O3} = -k_B T \ln\left(\frac{k_{O3 \rightarrow O2}}{k_{O2 \rightarrow O3}}\right)$$

$$(3)$$

At positive transmembrane potentials, the standard free energy $\Delta G_{O1 \rightarrow O2}$ increased with increasing KCl concentration in the chamber (Figure 8, Supporting Information, Table S3). For example, at an applied transmembrane potential of +80 mV, $\Delta G_{O1 \rightarrow O2}$ was -2.6 ± 0.1 and -4.2 ± 0.6 $k_B T$ in 1 and 4 M KCl, respectively. Since we considered the open O_2 substate a reference for all changes of the energetic maxima and minima in response to experimental alterations, this finding suggests that increasing KCl concentration destabilizes the open O_1 substate with respect to the open O_2 substate. In contrast, the standard free energy $\Delta G_{O3 \rightarrow O2}$ decreased in 4 M KCl concentration in the chamber. Since, the $O_2 \leftrightarrow O_3$ transitions are not voltage dependent, we found that the average values of the $\Delta G_{O3 \rightarrow O2}$ standard free energy, in the range of the transmembrane potential of -80 to $+80$ mV, were -1.7 ± 0.2 and -0.3 ± 0.2 $k_B T$ in 1 and 4 M KCl, respectively. Finally, we found that the standard free energy $\Delta G_{O1 \rightarrow O2}$ is always greater than that value of $\Delta G_{O3 \rightarrow O2}$ for all conditions examined in this work.

■ DISCUSSION

In this paper, we describe a comparative analysis of several sets of single-channel electrical data on the kinetics and thermodynamics of the gating process of the OpdK protein pore from *P. aeruginosa*. This protein exhibits a discrete kinetics that undergoes a three-well, two-barrier free energy landscape. Applying harsh experimental conditions, such as high KCl concentration in
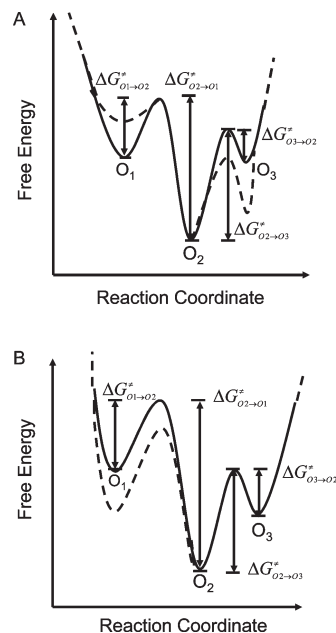
Figure 9. Alterations in the free energy landscape of the OpdK protein with modifications of the external conditions. (A) The free energy landscape at 1 M (continuous line) and 4 M (dashed line) KCl concentration. The applied transmembrane potential was +80 mV. (B) The free energy landscape for a transmembrane potential of +20 mV (continuous line) and +80 mV (dashed). The KCl concentration in the chamber was 1 M. The reaction coordinate indicates the positions of maxima and minima along the channel internal axis with respect to the periplasmic opening of the OpdK pore (Figure 1).

the chamber and applied transmembrane voltage did not modify the number of major wells or barriers that define the discrete kinetics of the OpdK protein. Moreover, we observed symmetry of the gating dynamics with respect to zero applied transmembrane potential (Figures 2−5), which is similar to most β-barrel membrane protein pores.[17−19] This symmetry of gating cannot be detected with voltage-gated channels, which undergo drastic conformational changes over a narrow voltage range.[59] Some β-barrel protein pores exhibit asymmetric gating dynamics in response to applied voltage.[6,60] The asymmetry in voltage dependence can also be observed with β-barrel porins reconstituted in liposomes containing membrane fractions that include lipopolysaccharides (LPS).[61]

Our three-state kinetic model is based upon a simple observation that there are three major open substates, O_1, O_2, and O_3, which are characterized by distinct current amplitudes (Figures 2−5; Supporting Information, Figures S2, S3, and S5). The total event probability of these major open substates, under all experimental conditions explored in this work, is at least ∼96%. Therefore, we adopted a three-state kinetic model (Supporting Information). Each open substate underwent a single-exponential distribution of the dwell time. Since in a Markovian system the number of exponentials is identical with the number of discrete substates,[51] the spontaneous stochastic gating of the OpdK protein follows a linear kinetic scheme. On the basis of this assessment, our qualitative and quantitative aspects of the spontaneous gating of the OpdK protein are relied on the time constants and event frequencies determined for the flanked open O_1 and O_3 substates (Supporting Information). To verify the correctness of this approach, we first determined the average τ_{O2} dwell times from

the histograms of the open O_2 substate, which is based on a model-independent determination. Independently, we then calculated the average τ_{O2} dwell times using the protocol based on eq 1, employing data extracted directly from the dwell-time histograms of the flanked open O_1 and O_3 substates. The latter value of the average τ_{O2} dwell time is based upon a model-dependent determination. Table 1 shows that these figures are closely similar, confirming the validity of the chosen three-state kinetic model. Assuming that the dwell times τ_{O1}, τ_{O2}, and τ_{O3} are identical, we estimated that the maximum errors of the kinetic rate constants $k_{O1\rightarrow O2}$, $k_{O2\rightarrow O1}$, $k_{O3\rightarrow O2}$, and $k_{O2\rightarrow O3}$, by omitting the contaminating channel substates, were 26, 0.8, 4.6, and 10 s^{-1}, respectively.

Our single-channel experiments with loop-deletion OpdK mutants provided a better understanding of the packing of long extracellular loops within the pore interior. OpdK ΔL3 showed a single-channel electrical signature similar to the WT-OpdK protein. This result contrasts our prior study with the OprD protein that indicated a direct participation of loop L3 to the pore constriction.[11] In this previous work, single-channel current recordings with a loop-deletion OprD ΔL3 mutant showed a drastic increase in unitary conductance, about 2-fold as compared to the wild-type OprD protein. We conclude that the Asp124-Pro129 region of L3 does not participate directly in the current fluctuations observed with the WT-OpdK protein. A different result was obtained with the OpdK ΔL7 protein, which exhibited a significant increase in the single-channel conductance (Figure 6). It should be noted that the OpdK ΔL7 protein removed an ion pair, Arg284-Asp116, between the L7 and L3 loops, respectively. These electrical recordings confirm the X-ray crystal structure of the OpdK protein that shows a direct participation of loop L7 to the constricted area of the pore lumen.

In Figure 7, we show the effects of the alterations in the KCl concentration and absolute applied transmembrane voltage on the three-state discrete kinetics of the OpdK protein pore. All free energy changes resulting from experimental alterations of the OpdK protein are with respect to a chosen reference, the most thermodynamically stable O_2 substate. At a transmembrane potential of +80 mV, increasing KCl concentration in the chamber from 1 to 4 M had a statistically significant impact on kinetic rate constants $k_{O1\rightarrow O2}$, $k_{O2\rightarrow O3}$, and $k_{O3\rightarrow O2}$. The KCl concentration-induced shift in the O_1 and O_3 minima produced an overall change of the standard free energies $\Delta G_{O1\rightarrow O2}$ and $\Delta G_{O3\rightarrow O2}$ (Figures 8 and 9, Supporting Information, Table S3).

We conclude that increasing KCl concentration to 4 M in the chamber results in a less energetically stable low-conductance open O_1 substate, but a more energetically stable large-conductance open O_3 substate, increasing the overall standard free energy $\Delta G_{O1\rightarrow O3}$. These alterations of the activation free energies might be attributable to electro-osmotic effect on the fluctuating polypeptide parts within the protein interior. It is likely that increasing KCl concentration in the chamber decreases the strength of the ion-pair interactions among the large extracellular loops, which otherwise have a stabilizing effect.[37,38] One example is the Asp116-Arg284 ion pair between loops L3 and L7, respectively. Rodrigues and colleagues reported that increasing KCl concentration in the chamber had a dramatic effect on the association and dissociation rate constants between neutral poly(ethylene glycol)s and the staphylococcal α-hemolysin (αHL) protein pore.[62] Increasing KCl concentration from 1 to 4 M, they found several hundred-fold increase in the association rate constants, whereas the dissociation rate constants decreased several hundred times.

Interestingly, increasing the absolute transmembrane voltage has no impact on the kinetic rate constants $k_{O2\rightarrow O3}$ and $k_{O3\rightarrow O2}$ (Figure 7A). This finding suggests that the part of the OpdK protein that undergoes this detectable conformational fluctuation, in the form of the low-amplitude current transitions, is not located within the high voltage drop of the pore interior. In contrast, increasing the applied transmembrane potential determined an enhancement of the $k_{O2\rightarrow O1}$ rate constant, decreasing the activation free energy $\Delta G^{\neq}_{O2\rightarrow O1}$ (Figures 7 and 9). We judge that increasing the applied voltage does not impair the energetic stability of the large-conductance open O_3 substate but catalyzes the frequency of the large-amplitude closures ($O_2 \rightarrow O_1$). The low-amplitude current transitions $O_2 \leftrightarrow O_3$ occurred with a very high frequency. This finding is in accord with a highly flexible movable part of the protein. In contrast, the large-amplitude closures occurred with a low frequency. Recent crystallographic work, along with single-channel electrical recording and site-directed mutagenesis, showed that an OprD ΔL3 deletion mutation of the structurally related OprD protein pore destabilized the polypeptide chain in the form of rapid current fluctuations.[11]

It should be noted that these experimental perturbations of the OpdK protein are not only followed by alterations of the thermal equilibrium among the three wells but also by modifications of the equilibrium within each of the wells. The former process is slow, involves thermally activated crossing barriers between wells, and has an exponential dependence on the barrier height. The latter process involves a much faster downhill Brownian diffusional transition,[63] which is not resolvable using our technique. Undoubtedly, the single-molecule dynamics of spontaneous gating of a β-barrel protein pore is a complex process that depends on a broad array of experimental factors, including the lipid composition of the monolayers,[61] the temperature,[26,32,64] the pH,[21,22,65-67] and the pore electrostatics.[17,29,34] In the future, a better understanding of spontaneous stochastic gating will be instrumental in the redesign of the β-barrel proteins that will potentially be used as stochastic sensor elements.[24,68-70]

Certainly, more experimentation, molecular engineering, and computational biophysics are required to obtain a better understanding of the functional properties and spontaneous gating dynamics of the OpdK protein. For example, temperature-dependent single-channel experiments[26,55] with loop deletion mutants would be instrumental in revealing the key mechanisms responsible for the stochastic motion of the extracellular loops within the pore interior. The precise nature of the gating transitions made by fluctuating loops might be determined by obtaining the enthalpic and entropic contributions to the kinetic and thermodynamic constants, revealing information about which process in the stochastic motion of the loops is dominant. It should be remembered that the conditions of our single-channel electrical recordings (e.g., the lipid composition of the membranes, the applied transmembrane potential, the ion concentration of the chamber) depart from the physiological environment of *P. aeruginosa*.[4,71] The single-channel current measured with OpdK protein in 150 mM KCl and at a transmembrane potential of several millivolts would not enable the detection of discernible and discrete open substates that can be altered by external changes of the system. We also executed single-channel electrical recordings with the OpdK protein in 500 mM KCl, which is much closer to the physiological conditions, and observed that the number of

major open substates (O_1, O_2, and O_3) is still conserved (Supporting Information, Figure S7). On the other hand, complementary molecular dynamics studies might be employed to examine the OpdK gating fluctuations under conditions that are much closer to the native features of the outer membranes of *P. aeruginosa*.

Since the high-resolution structure of this protein is now available,[10] one immediate question is how are these major open substates related to the OpdK structure? We speculate that the crystal structure should normally reflect the most thermodynamically stable conformation of the protein. In our case, the most stable conformation is the open O_2 substate. It is also true that the crystallization conditions depart from those experimental physical features of the reconstituted OpdK protein into the planar lipid bilayer. Nevertheless, it is unlikely that the structure of the OpdK channel should be related to the conformation of the open O_1 substate, since its probability is much lower than those values of the open O_2 and O_3 substates. Using MD simulations, Bond and colleagues found that the lipid bilayer environment and physiological salt concentrations contribute to alterations of the conformation of the extracellular loops in OpcA.[36]

In summary, we showed a simple model that accounts for the three major open substates of the OpdK protein pore, an OprD family member of *P. aeruginosa*.[10] We derived the kinetic and energetic constants based on a methodical approach of altering the KCl concentration in the chamber and changing the applied transmembrane potential. Our data indicate that the increase in the applied transmembrane potential had no effect on the low-amplitude current transitions but increases the frequency of the large-amplitude current closures. Single-channel data with loop-deletion mutants suggested a direct participation of loop L7 within the constriction of the pore lumen, which confirms the X-ray crystal structure of the OpdK protein. This work demonstrates that single-channel electrical recordings can be used to derive the alteration of the free energy landscape in response to drastic changes of experimental conditions, facilitating a better understanding of the wide range of discrete dynamical behaviors of protein channels and pores.

■ ASSOCIATED CONTENT

S **Supporting Information.** (i) Physical features of the extracellular loops of the OpdK protein, (ii) experimental evidence for the purity of *P. aeruginosa* OpdK used for single-channel electrical recordings, (iii) standard histograms of fitted current amplitudes, (iv) single-channel electrical trace of the native OpdK protein at a lower temperature, (v) temperature controller for single-channel electrical recordings with planar lipid bilayers, (vi) features of the loop-deletion OpdK mutants, (vii) single-channel electrical recordings with loop-deletion OpdK mutants, (viii) a three-state kinetic model for the current fluctuations of the wild-type OpdK protein, (ix) the standard free energies corresponding to various gating transitions of the wild-type OpdK protein, and (x) voltage dependence of the current amplitude of the discrete single-channel transitions. This material is available free of charge via the Internet at http://pubs.acs.org.

■ AUTHOR INFORMATION

Corresponding Author

*Ph 315-443-8078; Fax 315-443-9103; e-mail lmovilea@physics.syr.edu.

■ ACKNOWLEDGMENT

■ ABBREVIATIONS

FhuA, Ferric hydroxamate uptake component A of *E. coli*; MD, molecular dynamics; OM, outer membrane of Gram-negative bacteria; OmpA, outer membrane protein A of *E. coli*; OmpC, outer membrane protein C of *E. coli*; OmpF, outer membrane protein F of *E. coli*; OpcA, outer membrane protein A of *N. meningitidis*; OpdK, outer membrane protein K of *P. aeruginosa*; OprD, outer membrane protein D of *P. aeruginosa*; WT-OpdK, wild-type OpdK protein.

■ REFERENCES

(1) Trias, J., and Nikaido, H. (1990) Protein D2 channel of the Pseudomonas aeruginosa outer membrane has a binding site for basic amino acids and peptides. *J. Biol. Chem. 265*, 15680–15684.

(2) Ishii, J., and Nakae, T. (1993) Lipopolysaccharide promoted opening of the porin channel. *FEBS Lett. 320*, 251–255.

(3) Hancock, R. E., and Brinkman, F. S. (2002) Function of pseudomonas porins in uptake and efflux. *Annu. Rev. Microbiol. 56*, 17–38.

(4) Nikaido, H. (2003) Molecular basis of bacterial outer membrane permeability revisited. *Microbiol. Mol. Biol. Rev. 67*, 593–656.

(5) Hancock, R. E. W., and Tamber, S. (2004) Porins of the Outer Membrane of Pseudomonas aeruginosa in *Bacterial and Eukaryotic Porins: Structure, Function, Mechanism* (Benz, R., Ed.) pp 61−77, Wiley-VCH, Weinheim.

(6) Nestorovich, E. M., Sugawara, E., Nikaido, H., and Bezrukov, S. M. (2006) Pseudomonas aeruginosa porin OprF: properties of the channel. *J. Biol. Chem. 281*, 16230–16237.

(7) Sugawara, E., Nestorovich, E. M., Bezrukov, S. M., and Nikaido, H. (2006) Pseudomonas aeruginosa porin OprF exists in two different conformations. *J. Biol. Chem. 281*, 16220–16229.

(8) Tamber, S., Ochs, M. M., and Hancock, R. E. (2006) Role of the novel OprD family of porins in nutrient uptake in Pseudomonas aeruginosa. *J. Bacteriol. 188*, 45–54.

(9) Tamber, S., Maier, E., Benz, R., and Hancock, R. E. (2007) Characterization of OpdH, a Pseudomonas aeruginosa porin involved in the uptake of tricarboxylates. *J. Bacteriol. 189*, 929–939.

(10) Biswas, S., Mohammad, M. M., Movileanu, L., and van den Berg, B. (2008) Crystal structure of the outer membrane protein OpdK from Pseudomonas aeruginosa. *Structure 16*, 1027–1035.

(11) Biswas, S., Mohammad, M. M., Patel, D. R., Movileanu, L., and van den Berg, B. (2007) Structural insight into OprD substrate specificity. *Nat. Struct. Mol. Biol. 14*, 1108–1109.

(12) Ochs, M. M., Lu, C. D., Hancock, R. E., and Abdelal, A. T. (1999) Amino acid-mediated induction of the basic amino acid-specific outer membrane porin OprD from Pseudomonas aeruginosa. *J. Bacteriol. 181*, 5426–5432.

(13) Tamber, S., and Hancock, R. E. (2006) Involvement of two related porins, OprD and OpdP, in the uptake of arginine by Pseudomonas aeruginosa. *FEMS Microbiol. Lett. 260*, 23–29.

(14) Lauger, P. (1988) Internal motions in proteins and gating kinetics of ionic channels. *Biophys. J. 53*, 877–884.

(15) Kullman, L., Gurnev, P. A., Winterhalter, M., and Bezrukov, S. M. (2006) Functional subconformations in protein folding: evidence from single-channel experiments. *Phys. Rev. Lett. 96*, 038101.

(16) Phale, P. S., Schirmer, T., Prilipov, A., Lou, K. L., Hardmeyer, A., and Rosenbusch, J. P. (1997) Voltage gating of Escherichia coli porin channels: role of the constriction loop. *Proc. Natl. Acad. Sci. U.S.A 94*, 6741–6745.

(17) Van Gelder, P., Saint, N., Phale, P., Eppens, E. F., Prilipov, A., van, B. R., Rosenbusch, J. P., and Tommassen, J. (1997) Voltage sensing in the PhoE and OmpF outer membrane porins of Escherichia coli: role of charged residues. *J. Mol. Biol. 269*, 468–472.

(18) Bainbridge, G., Gokce, I., and Lakey, J. H. (1998) Voltage gating is a fundamental feature of porin and toxin beta-barrel membrane channels. *FEBS Lett. 431*, 305–308.

(19) Bainbridge, G., Mobasheri, H., Armstrong, G. A., Lea, E. J. A., and Lakey, J. H. (1998) Voltage-gating of Escherichia coli porin: A cystine-scanning mutagenesis study of loop 3. *J. Mol. Biol. 275*, 171–176.

(20) Liu, N., and Delcour, A. H. (1998) The spontaneous gating activity of OmpC porin is affected by mutations of a putative hydrogen bond network or of a salt bridge between the L3 loop and the barrel. *Protein Eng. 11*, 797–802.

(21) Robertson, K. M., and Tieleman, D. P. (2002) Molecular basis of voltage gating of OmpF porin. *Biochem. Cell Biol. 80*, 517–523.

(22) Delcour, A. H. (2003) Solute uptake through general porins. *Front Biosci. 8*, d1055–d1071.

(23) Basle, A., Iyer, R., and Delcour, A. H. (2004) Subconductance states in OmpF gating. *Biochim. Biophys. Acta 1664*, 100–107.

(24) Mapingire, O. S., Henderson, N. S., Duret, G., Thanassi, D. G., and Delcour, A. H. (2009) Modulating effects of the plug, helix, and N- and C-terminal domains on channel properties of the PapC usher. *J. Biol. Chem. 284*, 36324–36333.

(25) Phale, P. S., Philippsen, A., Widmer, C., Phale, V. P., Rosenbusch, J. P., and Schirmer, T. (2001) Role of charged residues at the OmpF porin channel constriction probed by mutagenesis and simulation. *Biochemistry 40*, 6319–6325.

(26) Chimerel, C., Movileanu, L., Pezeshki, S., Winterhalter, M., and Kleinekathofer, U. (2008) Transport at the nanoscale: Temperature dependance of ion conductance. *Eur. Biophys. J. 38*, 121–125.

(27) Mohammad, M. M., Howard, K. R., and Movileanu, L. (2011) Redesign of a plugged beta-barrel membrane protein. *J. Biol. Chem. 286*, 8000–8013.

(28) Mohammad, M. M., Prakash, S., Matouschek, A., and Movileanu, L. (2008) Controlling a single protein in a nanopore through electrostatic traps. *J. Am. Chem. Soc. 130*, 4081–4088.

(29) Mohammad, M. M., and Movileanu, L. (2010) Impact of distant charge reversals within a robust beta-barrel protein pore. *J. Phys. Chem. B 114*, 8750–8759.

(30) Liu, N., Samartzidou, H., Lee, K. W., Briggs, J. M., and Delcour, A. H. (2000) Effects of pore mutations and permeant ion concentration on the spontaneous gating activity of OmpC porin. *Protein Eng. 13*, 491–500.

(31) Basle, A., Qutub, R., Mehrazin, M., Wibbenmeyer, J., and Delcour, A. H. (2004) Deletions of single extracellular loops affect pH sensitivity, but not voltage dependence, of the Escherichia coli porin OmpF. *Protein Eng., Des. Sel. 17*, 665–672.

(32) Biro, I., Pezeshki, S., Weingart, H., Winterhalter, M., and Kleinekathofer, U. (2010) Comparing the temperature-dependent conductance of the two structurally similar E. coli porins OmpC and OmpF. *Biophys. J. 98*, 1830–1839.

(33) Wager, B., Basle, A., and Delcour, A. H. (2010) Disulfide bond tethering of extracellular loops does not affect the closure of OmpF porin at acidic pH. *Proteins 78*, 2886–2894.

(34) Choudhary, O. P., Ujwal, R., Kowallis, W., Coalson, R., Abramson, J., and Grabe, M. (2010) The electrostatics of VDAC: implications for selectivity and gating. *J. Mol. Biol. 396*, 580–592.

(35) Tieleman, D. P. (2006) Computer simulations of transport through membranes: passive diffusion, pores, channels and transporters. *Clin. Exp. Pharmacol. Physiol. 33*, 893–903.

(36) Bond, P. J., Derrick, J. P., and Sansom, M. S. (2007) Membrane simulations of OpcA: gating in the loops?. *Biophys. J. 92*, L23–L25.

(37) Luan, B., Caffrey, M., and Aksimentiev, A. (2007) Structure refinement of the OpcA adhesin using molecular dynamics. *Biophys. J. 93*, 3058–3069.

(38) Luan, B., Carr, R., Caffrey, M., and Aksimentiev, A. (2010) The effect of calcium on the conformation of cobalamin transporter BtuB. *Proteins 78*, 1153–1162.

(39) Faraldo-Gomez, J. D., Smith, G. R., and Sansom, M. S. (2003) Molecular dynamics simulations of the bacterial outer membrane protein FhuA: a comparative study of the ferrichrome-free and bound states. *Biophys. J. 85*, 1406–1420.

(40) Tian, P., and Bernstein, H. D. (2010) Molecular basis for the structural stability of an enclosed beta-barrel loop. *J. Mol. Biol. 402*, 475–489.

(41) Guzman, L. M., Belin, D., Carson, M. J., and Beckwith, J. (1995) Tight regulation, modulation, and high-level expression by vectors containing the arabinose PBAD promotor. *J. Bacteriol. 177*, 4121–4130.

(42) Movileanu, L., Neagoe, I., and Flonta, M. L. (2000) Interaction of the antioxidant flavonoid quercetin with planar lipid bilayers. *Int. J. Pharm. 205*, 135–146.

(43) Howorka, S., Movileanu, L., Lu, X. F., Magnon, M., Cheley, S., Braha, O., and Bayley, H. (2000) A protein pore with a single polymer chain tethered within the lumen. *J. Am. Chem. Soc. 122*, 2411–2416.

(44) Movileanu, L., and Bayley, H. (2001) Partitioning of a polymer into a nanoscopic protein pore obeys a simple scaling law. *Proc. Natl. Acad. Sci. U.S.A. 98*, 10137–10141.

(45) Movileanu, L., Cheley, S., Howorka, S., Braha, O., and Bayley, H. (2001) Location of a constriction in the lumen of a transmembrane pore by targeted covalent attachment of polymer molecules. *J. Gen. Physiol. 117*, 239–251.

(46) Colquhoun, D., and Sigworth, F. J. (1995) Fitting and statistical analysis of single-channel records in *Single-Channel Recording* (Sackmann, B. N. E., Ed.) 2nd ed., pp 483–587, Plenum Press, New York.

(47) McManus, O. B., Blatz, A. L., and Magleby, K. L. (1987) Sampling, Log Binning, Fitting, and Plotting Durations of Open and Shut Intervals From Single Channels and the Effects of Noise. *Pflugers Arch. 410*, 530–553.

(48) McManus, O. B., and Magleby, K. L. (1988) Kinetic states and modes of single large-conductance calcium-activated potassium channels in cultured rat skeletal-muscle. *J. Physiol. (London) 402*, 79–120.

(49) Movileanu, L., Cheley, S., and Bayley, H. (2003) Partitioning of individual flexible polymers into a nanoscopic protein pore. *Biophys. J. 85*, 897–910.

(50) Movileanu, L., Schmittschmitt, J. P., Scholtz, J. M., and Bayley, H. (2005) Interactions of the peptides with a protein pore. *Biophys. J. 89*, 1030–1045.

(51) Moss, G. W. J., and Moczydlowski, E. (2002) Concepts of single-channel analysis: inferring function from fluctuations in *Ion Channels - A Practical Approach* (Ashley, R. H., Ed.) 2nd ed., pp 69–112, Oxford University Press, Oxford.

(52) Wolfe, A. J., Mohammad, M. M., Cheley, S., Bayley, H., and Movileanu, L. (2007) Catalyzing the translocation of polypeptides through attractive interactions. *J. Am. Chem. Soc. 129*, 14034–14041.

(53) Goodrich, C. P., Kirmizialtin, S., Huyghues-Despointes, B. M., Zhu, A. P., Scholtz, J. M., Makarov, D. E., and Movileanu, L. (2007) Single-molecule electrophoresis of beta-hairpin peptides by electrical recordings and Langevin dynamics simulations. *J. Phys. Chem. B 111*, 3332–3335.

(54) Hanggi, P., Talkner, P., and Borkovec, M. (1990) Reaction-Rate Theory - 50 Years After Kramers. *Rev. Mod. Phys. 62*, 251–341.

(55) Mohammad, M. M., and Movileanu, L. (2008) Excursion of a single polypeptide into a protein pore: simple physics, but complicated biology. *Eur. Biophys. J. 37*, 913–925.

(56) Niedzwiecki, D. J., Grazul, J., and Movileanu, L. (2010) Single-molecule observation of protein adsoption onto an inorganic surface. *J. Am. Chem. Soc. 132*, 10816–10822.

(57) Movileanu, L., Benevides, J. M., and Thomas, G. J. (2002) Determination of base and backbone contributions to the thermodynamics

of premelting and melting transitions in B DNA. *Nucleic Acids Res.* 30, 3767–3777.

(58) Bikwemu, R., Wolfe, A. J., Xing, X., and Movileanu, L. (2010) Facilitated translocation of polypeptides through a single nanopore. *J. Phys.: Condens. Matter 22*, 454117.

(59) Roux, B., Allen, T., Berneche, S., and Im, W. (2004) Theoretical and computational models of biological ion channels. *Q. Rev. Biophys.* 37, 15–103.

(60) Miles, G., Movileanu, L., and Bayley, H. (2002) Subunit composition of a bicomponent toxin: Staphylococcal leukocidin forms an octameric transmembrane pore. *Protein Sci. 11*, 894–902.

(61) Samartzidou, H., and Delcour, A. H. (1998) E.coli PhoE porin has an opposite voltage-dependence to the homologous OmpF. *EMBO J. 17*, 93–100.

(62) Rodrigues, C. G., Machado, D. C., Chevtchenko, S. F., and Krasilnikov, O. V. (2008) Mechanism of KCl enhancement in detection of nonionic polymers by nanopore sensors. *Biophys. J. 95*, 5186–5192.

(63) Qian, H. (2002) From discrete protein kinetics to continuous Brownian dynamics: a new perspective. *Protein Sci. 11*, 1–5.

(64) Jung, Y., Bayley, H., and Movileanu, L. (2006) Temperature-responsive protein pores. *J. Am. Chem. Soc. 128*, 15332–15340.

(65) Nestorovich, E. M., Rostovtseva, T. K., and Bezrukov, S. M. (2003) Residue ionization and ion transport through OmpF channels. *Biophys. J. 85*, 3718–3729.

(66) Mari, S. A., Koster, S., Bippes, C. A., Yildiz, O., Kuhlbrandt, W., and Muller, D. J. (2010) pH-induced conformational change of the beta-barrel-forming protein OmpG reconstituted into native E. coli lipids. *J. Mol. Biol. 396*, 610–616.

(67) Damaghi, M., Bippes, C., Koster, S., Yildiz, O., Mari, S. A., Kuhlbrandt, W., and Muller, D. J. (2010) pH-dependent interactions guide the folding and gate the transmembrane pore of the beta-barrel membrane protein OmpG. *J. Mol. Biol. 397*, 878–882.

(68) Movileanu, L. (2008) Squeezing a single polypeptide through a nanopore. *Soft Matter 4*, 925–931.

(69) Movileanu, L. (2009) Interrogating single proteins through nanopores: challenges and opportunities. *Trends Biotechnol. 27*, 333–341.

(70) Wendell, D., Jing, P., Geng, J., Subramaniam, V., Lee, T. J., Montemagno, C., and Guo, P. (2009) Translocation of double-stranded DNA through membrane-adapted phi29 motor protein nanopores. *Nature Nanotechnol. 4*, 765–772.

(71) Sen, K., Hellman, J., and Nikaido, H. (1988) Porin channels in intact cells of Escherichia coli are not affected by Donnan potentials across the outer membrane. *J. Biol. Chem. 263*, 1182–1187.